Electronic Supplementary Material (ESI) for Organic & Biomolecular Chemistry.
This journal is © The Royal Society of Chemistry 2015

***OBC* manuscript OB-ART-11-2015-002371**

REVISED Version: 14 December 2015

Supporting Information

Structure of Olefin-Imidacloprid and Gas-phase Fragmentation Chemistry of its Protonated Form.

Roberto Fusetto, Jonathon White, Craig Hutton and Richard A. J. O'Hair*

School of Chemistry, Bio21 Institute of Molecular Science and Biotechnology, and ARC Centre of Excellence for Free Radical Chemistry and Biotechnology, University of Melbourne, Melbourne, Victoria, 3010, Australia

* Author to whom correspondence should be addressed: rohair@unimelb.edu.au

Synthesis of olefin-imidacloprid (2).

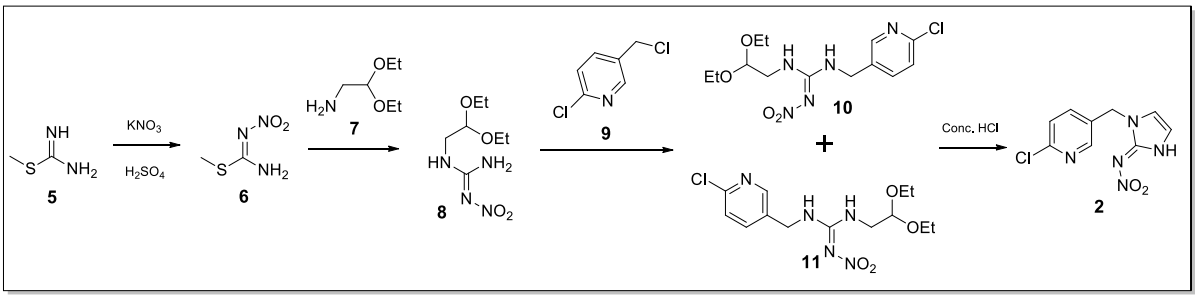

Scheme S1. Synthetic method used for the preparation of olefin-imidacloprid, **2**.

N-Nitro-S-methylisothiourea (6). 8.7 g of KNO_3 (86.2 mmol) was suspended in 22 mL of concentrated H_2SO_4 (98%). The reaction flask was cooled to -10°C in an ice bath then 12.0 g of S-methylisothiouronium sulphate (**5**, 43.1mmol) was added. The resulting mixture was stirred at 0°C for 2 hours. The mixture was neutralized with 1N NaOH and the precipitate isolated through suction filtration. The final product was dried under vacuum overnight to give **6** (5.3 g, 39.2 mmol, 45%) as a white powder; TLC (Hexane:EtOAc 4:6) $R_f = 0.45$; ^1H NMR ($CDCl_3$) δ 2.80 (3H, s, CH_3), 8.70 (2H, br s, NH_2); HRMS (ESI): $[M+H]^+$ *m/z* 136.0178; expected 136.0175.

N-(2,2-Diethoxyethyl)-N'-nitroguanidine (8). 5.3 g of **6** (39.2 mmol) was suspended in 30 mL of water and the mixture was stirred for 10 minutes before the dropwise addition of 5.7 mL of 2,2-diethoxyethanamine (**7**, 5.22 g, 39.2 mmol). The mixture was stirred at room temperature for 30 minutes. The insoluble product was collected through suction filtration and dried under vacuum overnight to yield 6.8 g of **8** (30.9 mmol, 79%) as a white powder. No purification was necessary.

38 TLC (Hexane:EtOAc 4:6) R_f = 0.15; ^{1}H NMR ($CDCl_3$) δ 1.25 (6H, t, J=7 Hz, 2 CH_3), 3.43 (2H,
39 dd, J=6.4 and 5 Hz, CH_2), 3.59 (2H, m, OCH_2), 3.76 (2H, m, OCH_2), 4.54 (1H, t, J=4.9 Hz, CH),
40 9.10 (2H, br s, NH); HRMS (ESI): $[M+H]^+$ *m/z* 221.12485; expected 221.12443.
41
42 ***N-(6-Chloropyridin-3-ylmethyl)-N'-(2,2-diethoxyethyl)-N''-nitroguanidine (10,11).*** To a
43 stirred solution of acetonitrile (160 mL) was added 8.8 g of K_2CO_3 (63.7 mmol) and 2.95 g of 2-
44 chloro-5-chloromethylpyridine (**9**, 18.2 mmol). The mixture was heated at 85°C for 20 hours.
45 The colour of the reaction changed from red to yellow. The acetonitrile was evaporated *in vacuo*
46 and the products extracted with EtOAc. The organic phase was washed three times with water
47 and brine, evaporated *in vacuo* and then the residue chromatographed with Hexane:EtOAc 2:8.
48 The two products **10** and **11** were collected together as a yellow oil in a yield of 2.9 g (46%).
49 TLC (EtOEt:EtOAc 9:1) (**10**) R_f = 0.40 (**11**) R_f = 0.32. ^{1}H NMR ($CDCl_3$) δ 1.23 (6H, m, 2 CH_3),
50 3.36 (2H, d, J=4.2 Hz, CH_2), 3.55 (2H, m, OCH_2), 3.75 (2H, m, OCH_2), 4.55 (1H, t, J=4 Hz,
51 CH), 4.73 (2H, s, CH), 7.33 (1H, d, J=8.2 Hz, C(5')H), 7.77 (1H, dd, J=8.2 and 1.8 Hz, C(4')H) ,
52 8.26 (1H, d, J=1.9 Hz, C(2')H); HRMS (ESI): $[M+H]^+$ *m/z* 346.12714; expected 346.12766.
53
54 ***N'-(6-Chloropyridin-3-ylmethyl)-N-nitro-1H-imidazol-2-ylamine (2).*** 2.9 g of a mixture of **10**
55 and **11** was stirred at room temperature in 20 mL of concentrated HCl for three days. The
56 product was extracted with DCM and washed with a solution of concentrated $NaHCO_3$, water
57 and brine. A slow evaporation of the solvent allowed the precipitation of the final product **2** as an
58 orange powder, 330 mg (15%).
59 TLC (Hexane:EtOAc 2:8) R_f = 0.1; ^{1}H NMR (DMSO-d_6) δ 5.11 (2H, s, CH_2), 7.05 (1H, s,
60 C(5)H), 7.33 (1H, s, C(4)H), 7.48 (1H, d, J=8.2 Hz, C(5')H), 7.73 (1H, dd, J=8.4 and 2.5 Hz,

C(4')H), 8.37 (1H, d, J=2.5 Hz, C(2')H), 12.74 (1H, br s, NH); HRMS (ESI): $[M+H]^+$ *m/z* 254.04397; expected 254.04393.

Distances			Angles		
	Crystal	Gas-phase		Crystal	Gas-phase
C(1)-N(3)	1.347(4)	1.366(9)	**N(3)-C(1)-N(1)**	107.1(2)	106.1(5)
C(1)-N(2)	1.355(3)	1.332(4)	**N(1)-C(1)-N(2)**	133.7(3)	133.4(9)
C(2)-N(1)	1.388(4)	1.387(5)	**C(3)-C(2)-N(1)**	108.0(2)	106.9(5)
C(4)-N(3)	1.454(3)	1.469(9)	**N(4)-N(2)-C(1)**	116.8(2)	117.1(7)
N(2)-N(4)	1.327(3)	1.364(1)	**C(1)-N(3)-C(4)**	123.4(2)	124.2(6)
N(4)-O(2)	1.249(3)	1.222(0)	**O(1)-N(4)-O(2)**	121.2(2)	123.0(3)
C(1)-N(1)	1.350(3)	1.357(9)	**O(1)-N(4)-N(2)**	122.4(2)	120.9(4)
C(2)-C(3)	1.346(4)	1.352(4)	**N(3)-C(1)-N(2)**	119.1(2)	120.3(5)
C(3)-N(3)	1.386(3)	1.392(0)	**C(3)-C(2)-N(1)**	108.0(2)	106.9(5)
C(4)-C(5)	1.515(4)	1.512(2)	**C(2)-C(3)-N(3)**	106.6(2)	107.6(2)
N(4)-O(1)	1.246(3)	1.254(3)	**C(1)-N(3)-C(3)**	109.7(2)	109.1(7)
Dihedral angles			**C(3)-N(3)-C(4)**	126.8(2)	126.5(6)
	Crystal	Gas-phase	**O(2)-N(4)-N(2)**	116.4(2)	116.0(1)
C(1)-N(2)-N(4)-O(1)	-0.6(4)	-0.8(1)			
N(1)-C(1)-N(2)-N(4)	-5.7(5)	-1.7(4)			
C(5)-C(4)-N(3)-C(3)	-99.7(3)	-88.9(0)			
N(3)-C(4)-C(5)-C(9)	28.3(3)	104.8(8)			
C(1)-N(2)-N(4)-O(2)	178.9(2)	178.9(4)			
C(5)-C(4)-N(3)-C(1)	84.2(3)	90.3(3)			
N(3)-C(4)-C(5)-C(6)	-159.9(4)	-75.5(6)			

Table S1. Distances, angles and dihedral angles of compound **2** in its crystal form and in the gas phase.

Ions	Formula of ion	Expected *m/z*	Measured *m/z*	Error (ppm)
2H$^+$	$C_9H_8ClN_5O_2$	254.04393	254.04367	1
4$^+$	$C_9H_6ClN_5O$	236.03336	236.03319	0.7
2H$_j^+$	$C_9H_8ClN_4$	208.05103	208.05084	0.9
2H$_i^+$	$C_9H_7ClN_4$	207.04320	207.04301	0.9

Table S2: HRMS measurements of **2H**$^+$ and its key fragment ions.

D-H...A	d(D-H) (Å)	d(H...A) (Å)	d(D...A) (Å)	<(DHA) (°)
N(1)-H...N(2)[i]	0.88(4)	2.62(3)	3.215(3)	126(3)
N(1)-H...O(1)[i]	0.88(4)	2.33(3)	3.002(3)	133(3)
N(1)-H...O(2)	0.88(4)	2.14(3)	2.590(3)	111(3)

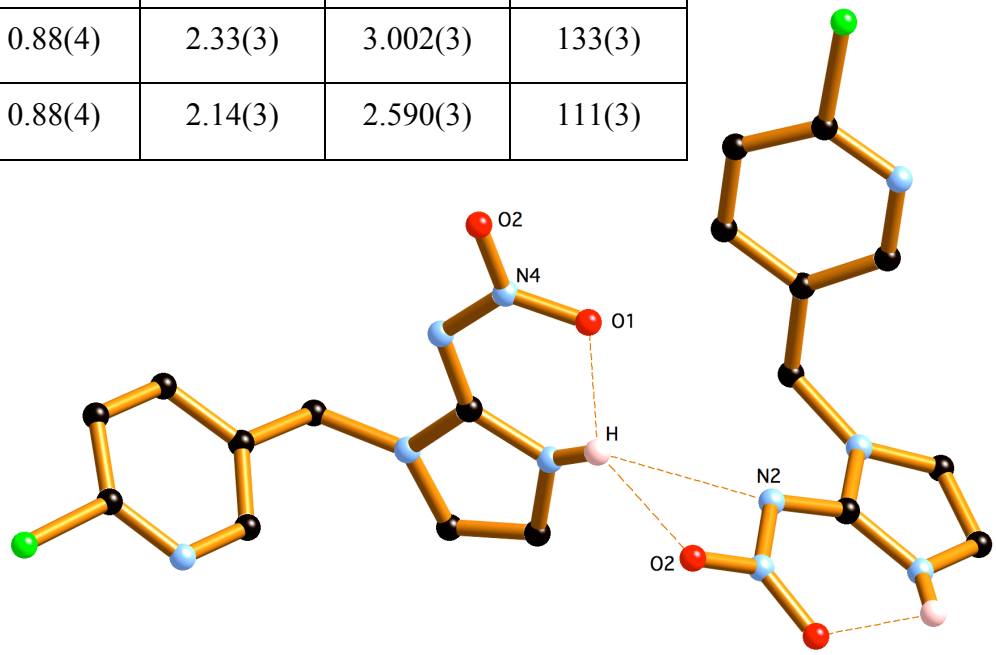

Figure S1. H-bonded chains extending along the z-direction and hydrogen bonds distances (Å) and angles (°). The crystal structure is characterized by both intramolecular N(1)-H…O(1) hydrogen bonds and intermolecular bifurcated N(1)-H...O(1) and N(1)-H…N(2) hydrogen bonds, which form infinite chains along the z-direction of the crystal. Symmetry transformations used to generate equivalent atoms: [i] x,-y+5/2,z+1/2.

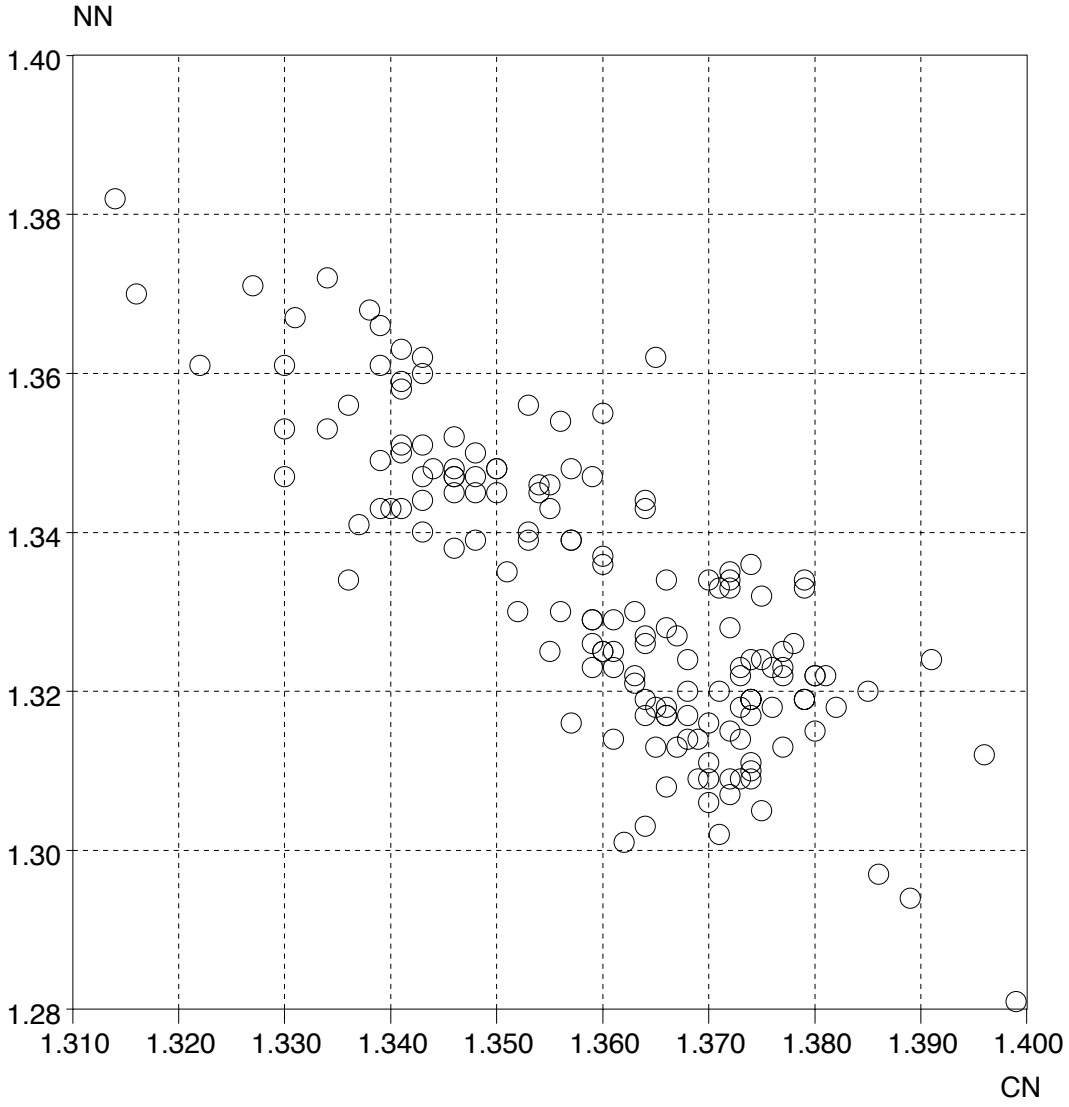

Figure S2. Scatter plot of the N-N distances *versus* the C-N distances for the two resonance forms A1 (top left) and A2 (bottom right). The structure represented by refcode AZECIR which has N-N of 1.281 Å and C-N of 1.399 Å resembles the resonance form A1. On the other extreme, the structure represented by the refcode QEVVIX which has N-N 1.382 Å and CN 1.314 Å resembles the resonance form A2. The remaining structures varied systematically between these two extremes.

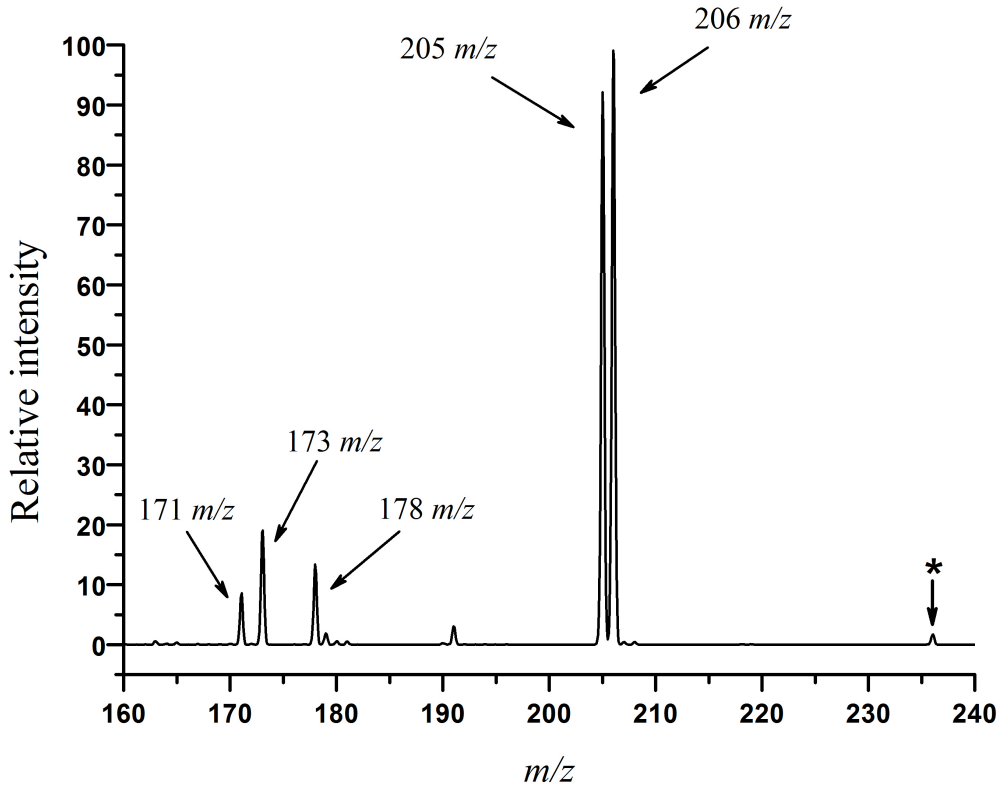

Figure S3. MS^3 of the product ion **4⁺(*)**, *m/z* 236 obtained using the linear ion trap with a normalized collision energy of 22% for 30 ms and a 1.0 *m/z* wide isolation window. The peaks at *m/z* 206 and 205 correspond to the loss of NO and HNO respectively. The structurally unidentified product ions at *m/z* 173 and 178 correspond to the losses of neutral(s) with overall formulas "N_2Cl" and "N_3O" respectively. The HRMS capabilities of the LTQ-FT permitted assignment of the molecular formulaes of these two product ions as: $C_9H_7ON_3$ (measured *m/z* 173.05827, 0.5 ppm error) and $C_9H_7N_2Cl$ (measured *m/z* 178.02915, 0.4 ppm error). The peak at *m/z* 171 corresponds to the loss of a chlorine atom from the product ion at *m/z* 206.

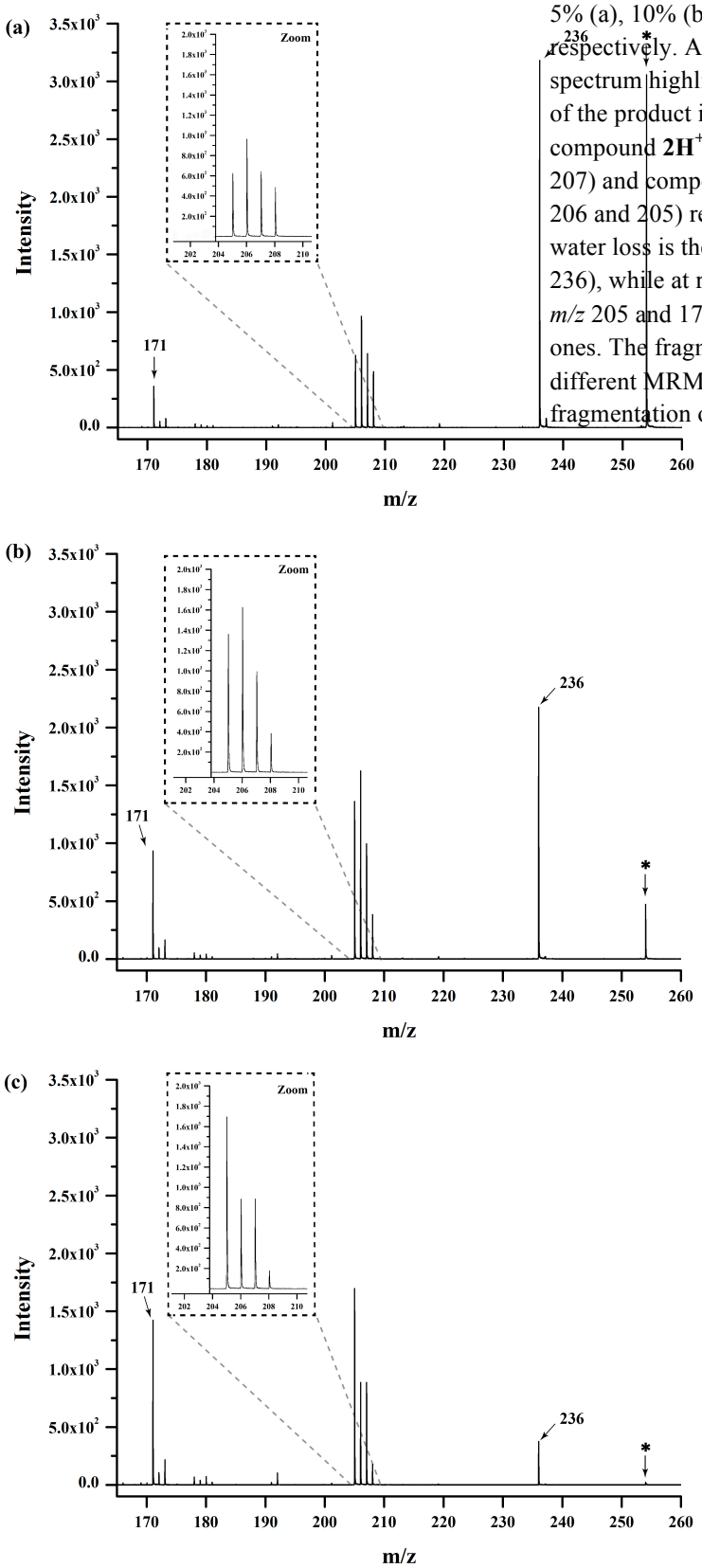

Figure S4. QTof CID mass spectra of mass selected **2H**$^+$ **(*)**, *m/z* 254 as a function of collision energy. Olefin-imidacloprid was mass selected with a window of 1.3 *m/z* and fragmented using 5% (a), 10% (b) and 15% (c) energy respectively. A zoom box in each spectrum highlight the different intensity of the product ions deriving from compound **2H**$^+$ (*m/z* 254→ *m/z* 208 and 207) and compound **4**$^+$ (*m/z* 236 → *m/z* 206 and 205) respectively. At low energy, water loss is the main product ion (*m/z* 236), while at rising energies the ions at *m/z* 205 and 171 become the predominant ones. The fragmented ions reported in the different MRM studies derive from the fragmentation of the main product ion **4**$^+$.

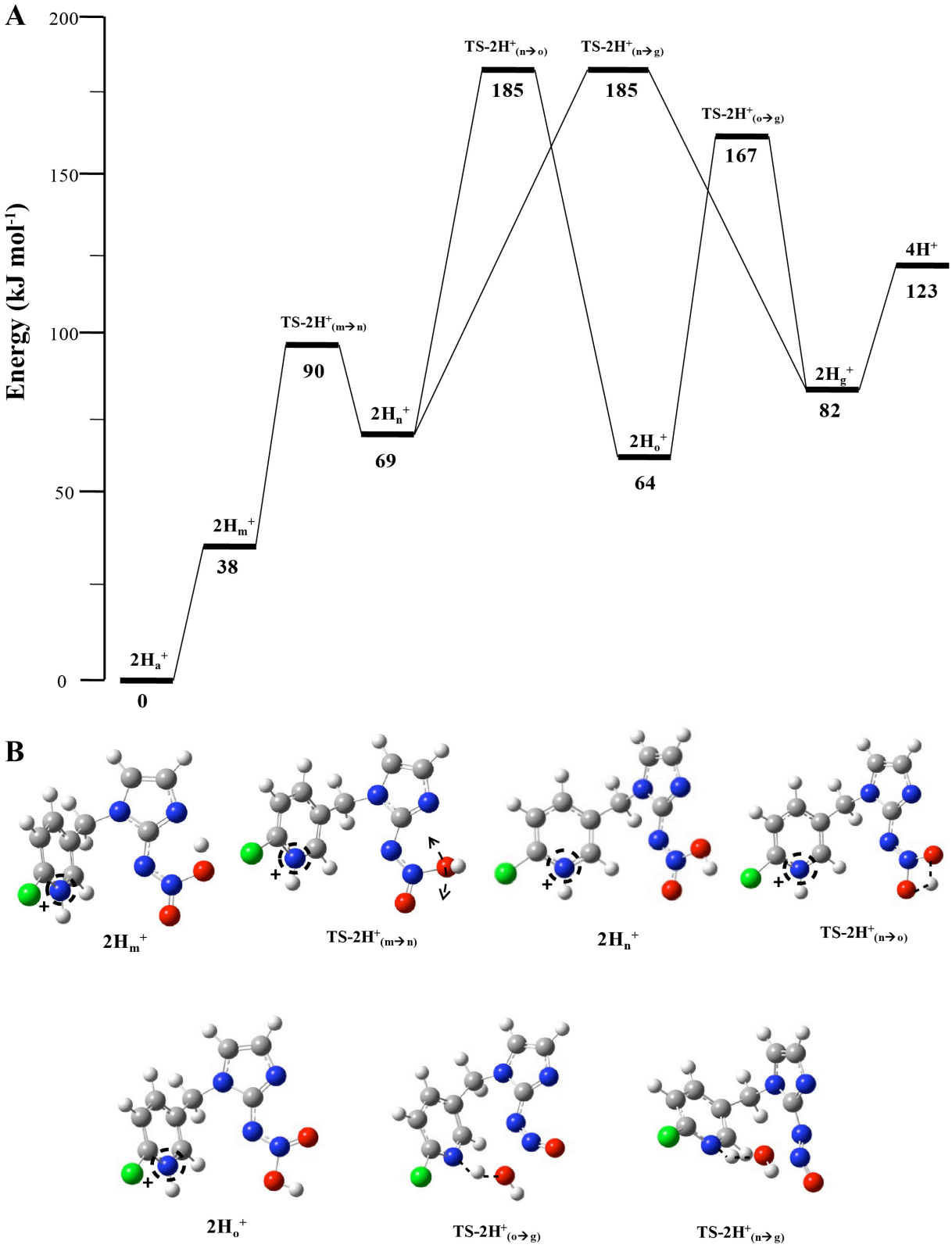

Figure S5. DFT calculated alternative, higher energy mechanisms for H_2O loss from **2H**$^+$: (A) Potential energy diagram. (B) Structures of key species.

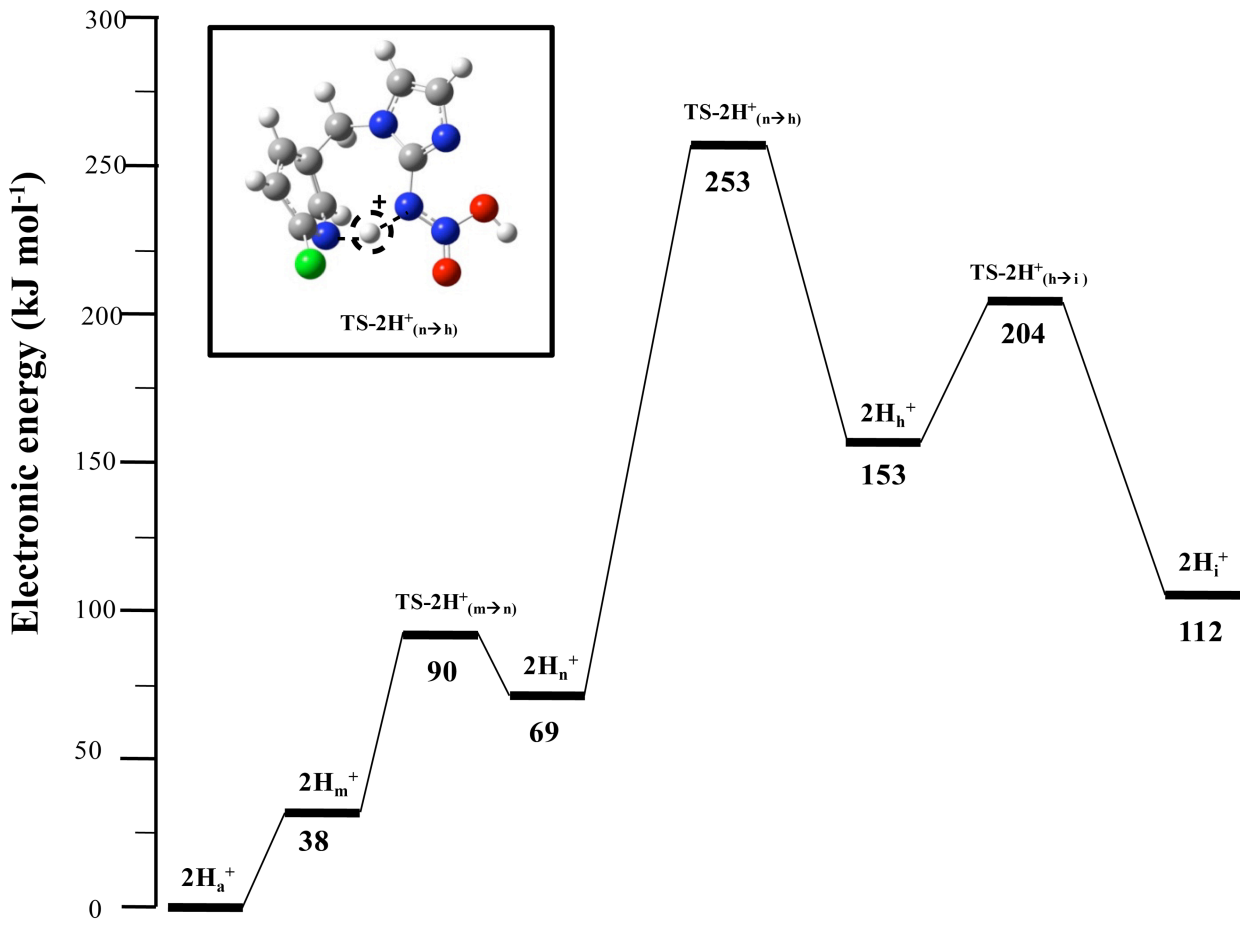

Figure S6. DFT calculated potential energy diagram alternative, higher energy mechanisms for HNO_2 loss from **2H**$^+$. Inset shows the key transition state TS-2H$^+_{(m\rightarrow h)}$.